It's risky to wander in September: Modelling the epidemic potential of Rift Valley fever in a Sahelian setting

Hélène Cecilia, Raphaëlle Métras, Assane Gueye Fall, Modou Moustapha Lo, Renaud Lancelot, Pauline Ezanno

It's risky to wander in September: Modelling the epidemic potential of Rift Valley fever in a Sahelian setting

Hélène Cecilia [a,b,c,]*, Raphaëlle Métras [d], Assane Gueye Fall [e], Modou Moustapha Lo [e], Renaud Lancelot [b,c], Pauline Ezanno [a]

[a] INRAE, Oniris, BIOEPAR, 44300, Nantes, France
[b] UMR ASTRE, CIRAD, Montpellier, France
[c] ASTRE, Montpellier University, CIRAD, INRAE, Montpellier, France
[d] Inserm, Sorbonne Université, Institut Pierre Louis d'Epidémiologie et de Santé Publique (IPLESP), F-75012, Paris, France
[e] Institut Sénégalais de Recherches Agricoles/Laboratoire National de l'Elevage et de Recherches Vétérinaires, BP 2057, Dakar-Hann, Senegal

A B S T R A C T

Estimating the epidemic potential of vector-borne diseases, along with the relative contribution of underlying mechanisms, is crucial for animal and human health worldwide. In West African Sahel, several outbreaks of Rift Valley fever (RVF) have occurred over the last decades, but uncertainty remains about the conditions necessary to trigger these outbreaks. We use the basic reproduction number (R_0) as a measure of RVF epidemic potential in northern Senegal, and map its value in two distinct ecosystems, namely the Ferlo and the Senegal River delta and valley. We consider three consecutive rainy seasons (July-November 2014, 2015 and 2016) and account for several vector and animal species. We parametrize our model with estimates of *Aedes vexans arabiensis*, *Culex poicilipes*, *Culex tritaeniorhynchus*, cattle, sheep and goat abundances. The impact of RVF virus introduction is assessed every week over northern Senegal. We highlight September as the period of highest epidemic potential in northern Senegal, resulting from distinct dynamics in the two study areas. Spatially, in the seasonal environment of the Ferlo, we observe that high-risk locations vary between years. We show that decreased vector densities do not greatly reduce R_0 and that cattle immunity has a greater impact on reducing transmission than small ruminant immunity. The host preferences of vectors and the temperature-dependent time interval between their blood meals are crucial parameters needing further biological investigations.

1. Introduction

Vector-borne diseases (VBDs) represent a growing threat to animal and human health worldwide. They account for 17 % of all infectious diseases, affecting more than one billion people each year (World Health Organization (WHO), 2014). Their presence in livestock can dramatically impact food production locally and hamper exports (Davies and Martin, 2003). This burden mostly affects low-income countries and their socio-economic development (World Health Organization (WHO), 2014). In addition, climate change, along with increased human and livestock mobility, create opportunities for vectors and their pathogens to establish in new areas, as was the case for West Nile virus in the United States of America (Calisher, 2000). Developing efficient countermeasures against VBDs requires a good understanding of their

transmission dynamics. This remains a major challenge considering the complexity of the biological system formed by pathogens, hosts, vectors and their relation to the environment (Parham et al., 2015).

Rift Valley fever virus (RVFV, Bunyaviridae: *Phlebovirus*) is a zoonotic and vector-borne pathogen, present throughout Africa, in the Arabian Peninsula and in the South West Indian Ocean islands. Mosquitoes of the Aedes and Culex genus are the main vectors (Chevalier et al., 2010), some of which are suspected to transmit the virus transovarially (Linthicum et al., 1985). They transmit it to a variety of domestic host species, including cattle, goats, sheep and camels, causing storms of abortions and a high mortality in young animals (Pepin et al., 2010). Human infection can occur through mucous membrane exposure or inhalation of viral particles (Davies and Martin, 2003). Most cases are limited to mild 'flu-like' symptoms (Laughlin et al., 1979), but severe

forms of the disease can be fatal. The case fatality rate is usually below 1 % (Madani et al., 2003) but tends to increase in recent outbreaks (Chevalier et al., 2010). Spillover into human population mainly concerns people working in close contact with animals such as pastoralists, butchers or veterinarians (Anyangu et al., 2010; Linthicum et al., 2016), but can be a concern for the general population, e.g. in a context of livestock slaughters during religious festivals (EMPRES, 2003; Lancelot et al., 2019). Vector-to-human transmission is possible but does not seem to be the major route of infection (Gerdes, 2004). Animal-to-animal transmission by direct contact seems possible but is not yet confirmed (Chevalier et al., 2010). Since 2015, RVF is part of the R&D Blueprint program of the World Health Organization (Mehand et al., 2018), a list of top emerging diseases likely to cause major epidemics, and for which few or no medical countermeasures exist.

Models are a powerful tool to explore pathogen transmission dynamics, and several approaches have already been used to answer questions about RVFV emergence and spread (Métras et al., 2011; Danzetta et al., 2016). Statistical models demonstrated an association between El Niño/Southern Oscillation phenomena and RVF occurrence in the Horn of Africa in 2007 (Anyamba et al., 2009), as well as the link between rainfall patterns and population dynamics of RVF vectors (Mondet et al., 2005). Network models highlighted factors influencing host mobility in regions affected by RVF (Apolloni et al., 2018; Kim et al., 2018; Belkhiria et al., 2019). The use of remote-sensing and geographic information systems (GIS) enabled the identification of landscape properties associated with RVF virus transmission (Tourre et al., 2009; Tran et al., 2016). However, prior to studying the transmission dynamics of a pathogen at large time- and spatial- scale, it is critical to understand the short-term consequences of its local introduction and in particular, its potential to trigger the onset of an epidemic.

The use of compartmental models together with the next generation matrix provides a way to estimate the basic reproduction number R_0 and gain a deeper understanding of the underlying processes contributing to the epidemic potential (Hartemink et al., 2008). R_0 represents the average number of secondary cases produced by one infected individual introduced in an entirely susceptible population over the course of its infectious period. Several mechanistic models have been proposed to formulate R_0 for RVF (Gaff et al., 2007; Niu et al., 2012; Xue and Scoglio, 2013; Pedro et al., 2016), but they remain theoretical and have not been applied in a spatially-explicit way using validated input data. In addition, R_0 is context-specific and studies mapping R_0 in space and time using data on hosts and vectors were primarily conducted for RVF-free regions, such as the Netherlands (Fischer et al., 2013) or the United States of America (Barker et al., 2013). In regions with regular RVF outbreaks, such as the West African Sahel, modelling R_0 could explain, upon a new introduction of the virus, what locally drives the rapid increase in RVF incidence and creates amplification hotspots.

Senegal and Mauritania have experienced several outbreaks since 1987. Most cases were reported in the Sahel region, more specifically in northern Senegal and southern Mauritania (Caminade et al., 2014; Sow et al., 2016). This region encompassing semi-arid to arid climate bridges the gap between the Sahara Desert and the tropical rainforests of equatorial Africa. In northern Senegal, RVF outbreaks have mainly been reported in two distinct ecosystems, along the Senegal River and in the Ferlo region. RVF epidemic potential is assumed to differ between these two study areas. Indeed, along the Senegal River, the availability of river water enabled the development of irrigated agriculture (Bruckmann, 2018), and therefore the continuous contact between vectors (mainly Culex) and hosts. In contrast, the Ferlo is much dryer. When the rainy season starts in July, temporary ponds are flooded. Aedes eggs, laid at the edges of ponds the year before, and which can resist desiccation, hatch and induce a rapid and massive emergence of adult mosquitoes (Ndione et al., 2008). In the meantime, vegetation grows and creates the suitable conditions for nomadic herds to stop along their transhumance pathway (Adriansen, 2008). Therefore, convergence of mosquitoes and

livestock, which are both capable of introducing the virus, create opportunities for RVF outbreaks.

Previous studies mapping RVF risk in West African Sahel overlapped climate anomalies and host densities, but they did not investigate the underlying mechanisms responsible for the disease outcome (Caminade et al., 2011, 2014). At very local scales, in particular around the village of Barkedji in the Ferlo region of Senegal, different approaches such as remote-sensing (Lacaux et al., 2007; Ndione et al., 2009) or statistical models (Bicout and Sabatier, 2004; Vignolles et al., 2009; Talla et al., 2016) were used. These studies focused on the link between landscape features (typically ponds, Soti et al., 2013; Bop et al., 2014) and vector abundance. Therefore, there is still a need for a mechanistic approach integrating all the major processes that may play a role in RVF epidemic potential.

The aim of the present paper is to map the epidemic potential of RVF virus in a Sahelian setting during the rainy season, comparing two different study areas, namely the Senegal River delta and valley, and the Ferlo. For this, we use an expression of R_0 in a multi-species (2 hosts and 2 vectors) context, accounting for vector feeding preferences. We identify parameters varying in time and space as well as relevant data sources to map contact zones between hosts and vectors. Next, the epidemic potential is quantified in independent spatial units, assuming each week of the rainy season to be a possible date of introduction, assessed separately. We identify locations and introduction times with higher epidemic potential. We assess the role of vector densities and herd immunity to reduce R_0. Eventually, we test the robustness of our results through a sensitivity analysis.

2. Material and methods

We built a compartmental, mechanistic model of RVF virus (RVFV) transmission with 2 host and 2 vector populations (Fig. 1, Eqs. S.1–S.3). We only included mechanisms accurately occurring at the onset of a potential epidemic, locally, upon the introduction of the virus, resulting from the introduction of an infected host or an infected vector. The model was used to obtain the next-generation matrix. We derived the expression of the basic reproduction number R_0 by using the method by van den Driessche and Watmough (2002), which averages the result of amplification following the two possible routes of virus introduction (infected host or infected vector, Supplementary Information 2). The value of R_0 was computed across each area (pixel resolution 3.5 km^2), and for weekly dates of virus introduction spanning three rainy seasons (July to November) of 2014, 2015, and 2016. These years corresponded to a period of evidenced RVFV circulation (Durand et al., 2020), along with the overlap of data source availability. Dates and location of RVFV introduction were assumed independent from each other. In addition, host infectious period is rather short (around a week) and temperatures did not strongly vary in our study area (interquartile range [29.1–31.4 °C], Fig. S.2) over the course of a vector lifetime (around a month). Thus, parameters were kept constant within each R_0 computation (i.e. each date and location of introduction) for the whole duration of secondary case generation, but were updated at each new computation.

2.1. Model structure and assumptions

Vectors were modelled using susceptible (S_i), latently infected (E_i), and infectious (I_i) health states, $i \in \{1,4\}$. In the Ferlo, vector species considered were *Aedes vexans arabiensis* (subscript 1) and *Culex poicilipes* (subscript 4). In the Senegal River delta and valley (SRDV), vector species considered were *Culex tritaeniorhynchus* (subscript 1) and *C. poicilipes* (subscript 4). This was based on previous entomological studies conducted in both areas (Diallo et al., 2011; Fall et al., 2011; Biteye et al., 2018). *Ae. v. arabiensis* and *C. poicilipes* are confirmed vectors of RVFV in Senegal (Fontenille et al., 1998; Diallo et al., 2000; Ndiaye et al., 2016). *C. tritaeniorhynchus* is highly abundant and was

A

B
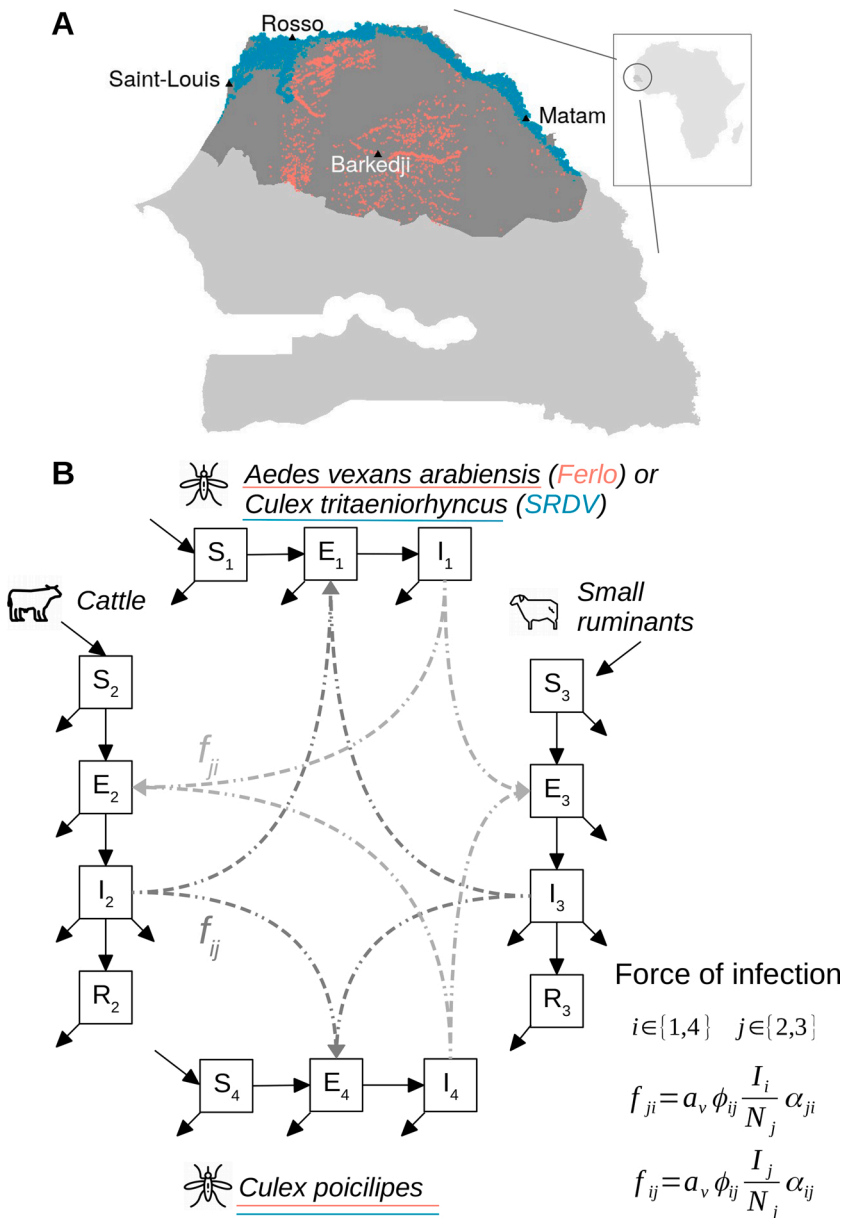
Fig. 1. Study area and model diagram. A – Study area, northern Senegal. Pixels highlighted correspond to locations with hosts and vectors at least once in the 3 rainy seasons, the color indicating the region and thus the vector species they contain. Ferlo (pink), n = 1702, Senegal River delta and valley (SRDV), n = 2676. B – Flow diagram of the RVFV mechanistic model used to obtain the next-generation matrix and derive the analytical formula of the basic reproduction number R_0. Formulas give the force of infection in host populations (from vectors) f_{ji} (light grey) and in vector populations (from hosts) f_{ij} (dark grey).

identified as a RVFV vector in the 2000 outbreak in Saudi Arabia (Jupp et al., 2002). In the model, vectors were assumed to become infected either after biting infectious cattle or small ruminants, but could not transmit the virus transovarially. Whilst limited evidence of vertical transmission of RVFV in mosquitoes is available (Linthicum et al., 1985), we assumed that this mechanism would be related to inter-annual patterns, rather than epidemic potential during a given rainy season (Lumley et al., 2017).

Host populations contained susceptible (S_j), latently infected (E_j), infectious (I_j), and recovered (with immunity, R_j) individuals, $j \in \{2,3\}$. They were stratified into cattle (subscript 2) and small ruminants (i.e. goats and sheep, subscript 3). Livestock could only be infected by the bites of infectious vectors. Animal-to-animal transmission by direct contact was here considered marginal compared to vector transmission, playing a minor role at the onset of a potential epidemic. Even though it might explain observed endemic patterns observed in unfavorable areas for mosquitoes (Nicolas et al., 2014), this transmission route has yet to be documented.

Mosquito biting rate, mortality and extrinsic incubation period (defined as the time between infection through a blood meal and virus

presence in the salivary glands) were assumed to be temperature-dependent for all vector species. In addition, we assumed that a proportion c_i of mosquito populations i could have double, partial, blood meals (Table 1, Supplementary Information 1.2). Transmission was modelled as reservoir frequency-dependent (Fig. 1, Eq. S.1), as defined by Wonham et al. (2006). In other words, an individual vector was considered to have a constant contact rate (biting rate + feeding preferences) with livestock populations regardless of surrounding host densities, whereas an individual host had a contact rate with vectors dependent on the vector-to-host ratio in the area (Gubbins et al., 2008). This type of transmission function can induce unrealistically high R_0 values when livestock densities are too low or vector densities are too high (Wonham et al., 2006). Therefore, for each introduction date, we removed pixels with vector-to-host ratio $(N_1 + N_4)/(N_2 + N_3) > 1000$. This threshold was chosen to significantly drop the highest values of R_0 without removing too many points (Table S.1). The force of infection included the relative preference of vectors for both livestock populations (π_{ij}, Table 1) combined with relative abundance of hosts to compute the proportion of blood meals taken on each host population (parameter ϕ_{ij}, Table 1). Parameter values and references are in Table 1, Supplementary

Table 1

Parameter values of the basic reproduction number R_0 derived from the mechanistic RVF virus transmission model with two host and two vector populations. Durations are in days, rates in days^{-1}. †: to the best of our knowledge. ECMWF: European Center for Medium Range Weather Forecasts.

	Definition	Value	Source
	Vector populations	subscripts $i \in \{1, 4\}$	
		$i = 1$: *Ae. v. arabiensis* (Ferlo),	
		C. tritaeniorhynchus (SRDV)	
		$i = 4$: *C. poicilipes*	
N_i	number of host-seeking female mosquitoes		Tran et al. (2019)
a_i	biting rate	$\dfrac{1 + c_i}{g_i(T)}$	
c_i	proportion of double blood meals	17 %	Ba et al. (2006)
$g_i(T)$	duration of gonotrophic cycle	$\dfrac{1}{(0.0173 \times (T - 9.6))}$	Madder et al. (1983)
$1/\varepsilon_i$	extrinsic incubation period	$\dfrac{1}{(0.0071T - 0.1038)}$	Barker et al. (2013)
ϕ_{ij}	proportion of blood meals taken on host population j	$\dfrac{\pi_{ij}N_j}{\pi_{i2}N_2 + \pi_{i3}N_3}, j \in \{2, 3\}, \pi_{i2} + \pi_{i3} = 1$	
π_{ij}	relative preference for host population j	0.843 for $j = 2$, 0.157 for $j = 3$	Ba et al. (2006)
$1/d_i$	vector lifespan	$\dfrac{1}{(0.000148T^2 - 0.00667T + 0.1)}$ $i = 1$, Ferlo	Tran et al. (2019)
		$\dfrac{1}{(0.000148T^2 - 0.00667T + 0.1) \times (1 - 0.016H)}$ $i = 1$, SRDV, $i = 4$	
	Host populations	subscripts $j \in \{2, 3\}$	
		$j = 2$: cattle $j = 3$: small ruminants	
N_j	Number of hosts		Gilbert et al. (2018)
p_j	proportion of immune individuals at disease-free equilibrium	0	
$1/\varepsilon_j$	incubation period	2	Spickler (2015)
$1/\gamma_j$	infectious period	6	Bird et al. (2009)
$1/d_j$	Host natural lifespan	$8 \times 365, j = 2$	†
		$2400, j = 3$	Hammami et al. (2016)
μ_j	RVF-induced mortality rate	0.0176 for $j = 2$, 0.0312 for $j = 3$	Gaff et al. (2007)
	Transmission	$i \in \{1, 4\}, j \in \{2, 3\}$	
α_{ij}	host-to-vector successful transmission probability	0.6	Cavalerie et al. (2015)
α_{ji}	vector-to-host successful transmission probability	0.4	Cavalerie et al. (2015)
T	temperature ($^\circ C$)	$(T_{min} + T_{max})/2$	T_{min}, T_{max} from ECMWF
H	relative humidity (%)	$100 \cdot \dfrac{exp\left(\dfrac{17.27(T_{min} - 2)}{(T_{min} - 2) + 237.3}\right)}{exp\left(\dfrac{17.27T_{max}}{T_{max} + 237.3}\right)}$	

information 1.2.

2.2. Input data

A schematic representation of data inclusion into our modelling framework, along with other parametrization aspects, can be found in Supplementary Information 1.2.

2.2.1. Spatio-temporal data on vector abundance

The vector abundance in space and time was derived from the predictions of a mechanistic model of mosquito population dynamics developed by Tran et al. (2019). This model provides the abundance of host-seeking female mosquitoes for the three vector species and the two regions of interest. Mosquito abundance is driven by rainfall, temperature, location of waterbodies, and the surface dynamics of ponds throughout the year. This model uses satellite-derived meteorological data and multispectral images to assess the habitat suitability for vectors. Tropical Applications of Meteorology using SATellite data (TAMSAT) daily rainfall estimates are used (http://www.tamsat.org.uk/cgi-bin/data/index.cgi), along with the European Centre for Medium Range Weather Forecasts (ECMWF) 10-daily minimum and maximum temperatures (https://confluence.ecmwf.int). Water bodies are detected using cloud-free Sentinel 2 scenes (level 1-C, https://earthexplorer.usgs.gov/). Their filling dynamics is estimated with an existing hydrologic model (Soti et al., 2010). The predictions of this model have been validated against entomological data collected in several sites in our study area (Biteye et al., 2018). We used weekly mosquito abundance for three consecutive rainy seasons (July to November 2014, 2015 and

2016, downloaded from https://doi.org/10.18167/DVN1/IQ2J1L). Our spatial units were hexagonal pixels of 1 km radius (≈ 3.5km^2) as in Tran et al. (2019).

2.2.2. Spatial distribution of livestock

For livestock host densities, we used the Gridded Livestock of the World database (GLW 3, downloaded from https://dataverse.harvard.edu/dataverse/glw_3, Gilbert et al., 2018), which provides subnational livestock distribution data for 2010, at a spatial resolution of 0,083333° (approximately 10 km at the equator). We used the distributions of cattle and small ruminants (goats and sheep) based on Gilbert et al. (2018) dasymetric product, which disaggregates census data according to weights established by statistical models using high resolution spatial covariates (land use, climate, vegetation, topography, human presence). This dataset was downscaled to match Tran et al. (2019) model pixel size by homogeneously distributing animals in smaller space units. The GLW 3 dataset is an average snapshot and does not provide time series of animal densities.

2.3. Analytical expression of the basic reproduction number

R_0 was computed only for pixels in which both hosts and vectors were present. We considered the chosen spatial resolution large enough to neglect vector dispersal among pixels, in agreement with entomological studies conducted in the Ferlo and SRDV which show that vectors rarely disperse further than 1 km from ponds (Ba et al., 2005; Diallo et al., 2011; Fall et al., 2013). In addition, quantitative information on seasonal variations in livestock abundance at large scale was not

available. As a result, we considered that pixels were disconnected and that animal densities remained constant.

R_0 is the dominant eigenvalue of the next generation matrix of our model (Eqs. 1–5). The details of its computation can be found in Supplementary Information 2. Compared to the expression derived by Turner et al. (2013) for bluetongue, we accounted for an incubation period, a natural mortality rate and a proportion of immune individuals at the disease-free equilibrium in livestock hosts. We also considered transmission probabilities (vector-to-host and host-to-vector) to be host-population specific and not only vector-population specific.

$$R_0 = \sqrt{\frac{1}{2}\left[(R_{11} + R_{44}) + \sqrt{(R_{11} + R_{44})^2 - 4(R_{11}R_{44} - R_{14}R_{41})}\right]} \quad (1)$$

$$R_{11} = \frac{\varepsilon_1}{(d_1 + \varepsilon_1)d_1} \times \left(\frac{\frac{N_1}{N_2}\varepsilon_2\alpha_{21}\alpha_{12}(\phi_{12}a_1)^2}{(d_2 + \varepsilon_2)(d_2 + \gamma_2 + \mu_2)}(1 - p_2) + \frac{\frac{N_1}{N_3}\varepsilon_3\alpha_{31}\alpha_{13}(\phi_{13}a_1)^2}{(d_3 + \varepsilon_3)(d_3 + \gamma_3 + \mu_3)}(1 - p_3)\right) \quad (2)$$

$$R_{44} = \frac{\varepsilon_4}{(d_4 + \varepsilon_4)d_4} \times \left(\frac{\frac{N_4}{N_2}\varepsilon_2\alpha_{24}\alpha_{42}(\phi_{42}a_4)^2}{(d_2 + \varepsilon_2)(d_2 + \gamma_2 + \mu_2)}(1 - p_2) + \frac{\frac{N_4}{N_3}\varepsilon_3\alpha_{34}\alpha_{43}(\phi_{43}a_4)^2}{(d_3 + \varepsilon_3)(d_3 + \gamma_3 + \mu_3)}(1 - p_3)\right) \quad (3)$$

$$R_{14} = \frac{\varepsilon_4}{(d_4 + \varepsilon_4)d_4} \times \left(\frac{\frac{N_1}{N_2}\varepsilon_2\alpha_{21}\alpha_{42}\phi_{12}\phi_{42}a_1a_4}{(d_2 + \varepsilon_2)(d_2 + \gamma_2 + \mu_2)}(1 - p_2) + \frac{\frac{N_1}{N_3}\varepsilon_3\alpha_{31}\alpha_{43}\phi_{13}\phi_{43}a_1a_4}{(d_3 + \varepsilon_3)(d_3 + \gamma_3 + \mu_3)}(1 - p_3)\right) \quad (4)$$

$$R_{41} = \frac{\varepsilon_1}{(d_1 + \varepsilon_1)d_1} \times \left(\frac{\frac{N_4}{N_2}\varepsilon_2\alpha_{24}\alpha_{12}\phi_{12}\phi_{42}a_1a_4}{(d_2 + \varepsilon_2)(d_2 + \gamma_2 + \mu_2)}(1 - p_2) + \frac{\frac{N_4}{N_3}\varepsilon_3\alpha_{34}\alpha_{13}\phi_{13}\phi_{43}a_1a_4}{(d_3 + \varepsilon_3)(d_3 + \gamma_3 + \mu_3)}(1 - p_3)\right) \quad (5)$$

### 2.4. Spatio-temporal pattern of R_0

First, we identified dates and locations of RVFV introduction with high epidemic potential. For each area under study, we examined which introduction date resulted in the highest number of pixels with $R_0 > 1$, each season. For clarity hereinafter, pxl_1 is the number of pixels with $R_0 > 1$ at a given introduction date. For each season, we computed an R_0 threshold corresponding to the value of the third quartile, independently of the study area and date of introduction within a given season, $Q_{3, year}$. We mapped pixels for which $R_0 > Q_{3, year}$ at least once within the season; we also recorded the number of times (i.e. weeks) it happened during the season. This was made to highlight high-risk areas. For two specific locations, namely Rosso in SRDV and Barkedji in the Ferlo, we normalized R_0 values (dividing them by the maximum R_0 value of the season) in order to compare seasonal patterns without focusing on absolute R_0 values.

We then investigated the role of vector and host populations on the epidemic potential. We inspected how the relative abundances of vector populations changed over time within pixels with $R_0 > 1$. We focused on three specific dates of virus introduction in Barkedji, in 2015. This was done to specifically understand whether lower vector densities (without any modification of their lifespan parameters) could significantly decrease R_0 values. We also aimed to identify which species had the most impact on R_0 when decreased, and whether this was influenced by the vector composition, quantified with $log_{10}(N_{C.\ poicilipes}/N_{Ae.\ v.\ arabiensis})$. The first date we chose corresponded to the maximum pxl_1 in the Ferlo over the season. The other two dates both induced $R_0 > 1$ in Barkedji but exhibited diametrically opposed vector composition. Similarly, we assessed the effect of herd immunity, which could be acquired either through vaccination or previous exposure to RVFV, on the number of pixels with $R_0 > Q_{3, year}$, per study area and season.

Finally, we performed a variance-based global sensitivity analysis
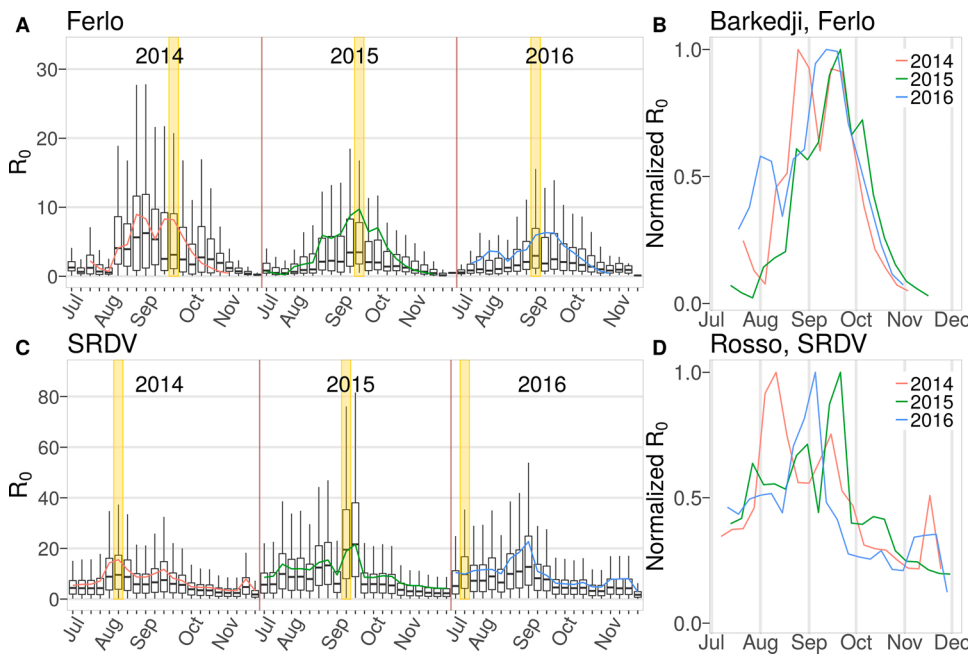
Fig. 2. September is the month of highest RVFV epidemic potential in northern Senegal. A, C: R_0 distribution by introduction date for 3 consecutive rainy seasons, spatially aggregated by region (A: Ferlo; C: SRDV). R_0 values are computed independently for each introduction date, assuming constant parameters over the course of the secondary case generation. Colored lines show the temporal patterns for Barkedji (Ferlo) and Rosso (SRDV). Yellow bands highlight the introduction dates inducing the highest number of pixels with $R_0 > 1$, for each rainy season. Northern Senegal (Ferlo + SRDV): 2014-09-22, n = 3557, 2015-09-14, n = 3944, 2016-09-05, n = 3411. Ferlo: 2014-09-22, n = 1313, 2015-09-21, n = 1527, 2016-09-05, n = 1022. SRDV: 2014-08-11, n = 2352, 2015-09-14, n = 2482, 2016-07-18, n = 2397. The median R_0 value is 1.51 in the Ferlo, 4.95 in SRDV. B, D: Comparison of yearly R_0 pattern for Barkedji and Rosso. Values are normalized by the maximum of each rainy season. In the boxplots, box boundaries indicate the 25th (bottom) and 75th (top) percentiles. The line within the box marks the median. Whiskers above and below the box indicate the 10th and 90th percentiles. Outliers outside the 10th and 90th percentiles are not shown to ease figure reading. (For interpretation of the references to colour in this figure legend, the reader is referred to the web version of this article).

using a Fourier Amplitude Sensitivity Testing (FAST, Saltelli et al., 2008). This method was used to quantify first order effects of parameters but also interactions between parameters varying simultaneously, which is not possible with ``one-at-a-time'' sensitivity analyses (Saltelli et al., 2019). Parameters varied within a 10 % range using scaling factors (reference value of 1). A given set (scenario) of scaling factors was applied to all R_0 computations of a given study area and rainy season, to maintain the spatial heterogeneity as well as the relative temporal dynamics of vector densities and temperature-dependent parameters. Temperature-dependent function formulas were kept, and temperature was not varied. We sampled 10,000 values per parameter. We tested whether introduction dates and locations with high epidemic potential were robust to these parameter variations.

3. Results

Overall, there are 2.5 times more R_0 values computed in the Senegal River delta and valley (SRDV) than in the Ferlo. Initially, input data covers a total surface of ~15,500 km^2, comprised of 4419 independent pixels (1702 in the Ferlo, 2717 in SRDV) containing both hosts and vectors at least once in the 63 introduction dates (21 per season) studied. Over the 235,449 possible R_0 computations, 3.7 % are discarded because the local vector-to-host ratio is too high (Supplementary Information 3). This mainly affects SRDV, where 41 pixels are entirely removed from the study because their ratio never goes below the chosen threshold during the 3 rainy seasons (Supplementary Information 3). We end up with a stable surface where R_0 is computed per time step in SRDV (between 90 % and 100 % of the possible surface available in the data), whereas this proportion largely varies within a season in the Ferlo (from 0.1 % to 100 %). In addition, the number of pixels with $R_0 > 1$ per introduction date (pxl_1) never goes below 1767 for any date of introduction in SRDV (always >66 % of R_0 computations in this study area), and reaches its absolute maximum on 2015-09-14 (n = 2482). In the Ferlo, pxl_1 can go from 0 for introductions in November (2014-11-24, 2015-11-30, 2016-11-21, and 2016-11-28) to 1527 (93 % of R_0 computations) on 2015-09-21.

September is the month of highest RVF epidemic potential in northern Senegal for the three studied rainy seasons. The two study areas exhibit different epidemic potential temporal patterns. In the Ferlo, the epidemic potential is seasonal (median $R_0 = 1.51$), and September is systematically highlighted as the period of highest RVFV epidemic potential (Fig. 2A) despite some variability in temperature and mosquito abundances between years (Figs. S.2, S.4). In the Senegal River delta and valley, the epidemic potential is high throughout the rainy seasons (median $R_0 = 4.95$), with overall 90 % of R_0 values above 2 in the whole studied period. The temporal pattern in two specific locations is similar to the one observed at the respective regional scale (Fig. 2). The pixel closest to Rosso has its $R_0 > 1$ for every possible date of introduction over the three consecutive rainy seasons, which is not the case for the pixel closest to Barkedji (Fig. 2A, C, colored lines).

In northern Senegal, for the three years studied, the introduction date of highest epidemic potential is reached earlier every year (2014-09-22, $pxl_1 = 3557$, 2015-09-14, $pxl_1 = 3944$, 2016-09-05, $pxl_1 = 3411$). This trend is robust to the parameter variations tested in our sensitivity analysis, as well as the dates of maximum pxl_1 within each study area (Table S.9).

The map of areas with highest epidemic potential varies across the three rainy seasons of 2014, 2015 and 2016 (Fig. 3). In the Ferlo, the south-west of Barkedji exhibits a high epidemic potential in 2014 but not in 2015–2016. Conversely, the north-east of Barkedji exhibits a high epidemic potential in 2015–2016 but not in 2014. In SRDV, around Matam, there is a strong density of pixels with R_0 above the third quartile of the season ($Q_{3, year}$) in 2015–2016 but less so in 2014. Overall, SRDV accounts for a larger proportion of pixels with $R_0 > Q_{3, year}$ than the Ferlo, every season (at least three times more, Table S.8). In addition, the frequency of these high R_0 values is lower per pixel in the Ferlo than in SRDV, every season (Fig. 3, pixels ranging from green to yellow, Table S.8). These results are also robust to parameter variations (Fig. S.9).

In the Ferlo, *Ae. v. arabiensis* tends to be the most abundant vector population within pixels with $R_0 > 1$ at the beginning of the rainy season, while *C. poicilipes* is the most abundant later in the season (Figs. 4A,
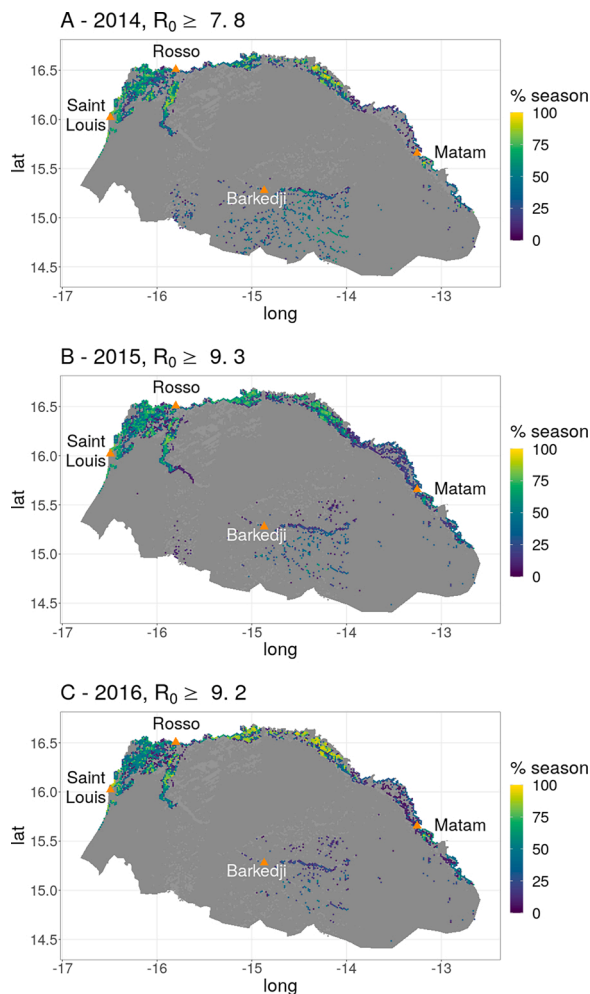
Fig. 3. Zones of high RVF epidemic potential change between rainy seasons. Map of northern Senegal showing pixels with $R_0 > Q_{3, year}$ (third quartile of R_0 values) at least once in the season. Pixels are colored by percentage of season spent above the threshold (1 to 21 weeks). Orange points are important locations to ease figure reading. Light grey pixels are other pixels where R_0 is computed during the season.

S.4). Nonetheless, the vector composition shows a large variability between pixels for a same date of introduction. For instance, on October 12th 2015, minimum and maximum relative abundances are $log_{10}(N_{C. poicilipes}/N_{Ae. v. arabiensis})$ =-3.74 and $log_{10}(N_{C. poicilipes}/N_{Ae. v. arabiensis})$ = 4.44 respectively (Fig. 4A). In addition, inspecting dates resulting in the highest pxl_1, *Ae. v. arabiensis* is on average the most abundant in pixels with $R_0 > 1$ in 2014 (2014-09-22, Fig. S.4), while *C. poicilipes* is on average the most abundant in pixels with $R_0 > 1$ in 2015 and 2016 (2015-09-21, 2016-09-05, Figs. 4A, S.4). In Barkedji, diametrically opposed vector compositions can induce $R_0 > 1$, such as August 24th 2015 when $log_{10}(N_{C. poicilipes}/N_{Ae. v. arabiensis})$ = -1.08 and October 12th 2015 when $log_{10}(N_{C. poicilipes}/N_{Ae. v. arabiensis})$ = 1.08 (Fig. 4A, B, D). In SRDV, *C. tritaeniorhynchus* is always the most abundant species in every pixel with $R_0 > 1$, but the gap between population densities is less important than in the Ferlo (Fig. S.4).

Decreased vector densities do not greatly reduce R_0 values of at-risk pixels below 1 (Fig. 4). In Barkedji, this is observed regardless of RVFV introduction date and whichever species is the most abundant. In addition, the vector composition is not an indicator of which population, if decreased, will more strongly affect R_0. Indeed, for RVFV introductions on August 24th 2015 and September 21st 2015, decreasing the density of the most abundant vector population has the strongest effect on R_0 value (Fig. 4A–C). This is not observed on October 12th

2015, when *C. poicilipes* are more numerous than *Ae. v. arabiensis* in Barkedji (Fig. 4A, third red star), but decreasing the density of *Ae. v. arabiensis* has the strongest impact on R_0 (Fig. 4D).

In both study areas, an increase in the proportion of immune cattle decreases the number of pixels with high R_0 values ($R_0 > Q_{3, year}$) more effectively than increasing the proportion of immune small ruminants (Figs. 5B, C, S.5). In most pixels (4302/4367 = 98.5%), the number of small ruminants is higher than the number of cattle (Fig. 5A). However, the difference in host populations sizes is smaller in SRDV than in the Ferlo. Indeed, there are on average 7.5 times more small ruminants than cattle in the Ferlo, and only twice more in SRDV. This is related to the presence of both very low cattle densities and very high small ruminant densities in the Ferlo, while the range of SRDV host distributions is narrower (Fig. S.3). As a consequence, cattle are in fewer numbers than small ruminants while being the preferred host of all vector species studied (Table 1, Supplementary information 1.2). Therefore, they are more likely to get bitten more than once. These bites, provided they result in successful transmission (first to the host, then to a vector), can strongly contribute to RVF epidemic potential.

Finally, the feeding preferences and the gonotrophic cycle duration of the most abundant vector species are the most influential parameters on the epidemic potential in the Ferlo (Figs. 6, S.6). In 2015, the first order effects of these parameters explain respectively 47 % and 19 % of the variance observed in the maximum pxl_1 of the season. In SRDV, the maximum pxl_1 does not vary much in our sensitivity analysis (maximum 2.4 % from the reference value in 2016, Fig. S.7), because it quickly reaches the total number of pixels where R_0 is computed for the study area. It is nonetheless influenced by the same parameters as highlighted for the Ferlo (Fig. S.7). Specifically, the more the feeding preference of the most abundant vector population is skewed towards cattle, and the more often these vectors have to take a new blood meal, the higher pxl_1.

4. Discussion

The results of our analyses show that an introduction of Rift Valley fever virus in September has the potential to trigger an epidemic almost everywhere in northern Senegal. In the Ferlo region, there is a clear seasonality of the epidemic potential, and the most at-risk ponds change between rainy seasons. In contrast, but as expected, the Senegal River delta and valley contains areas with high epidemic potential during most of the rainy season, as it is a persistent conducive vector habitat. In addition, the period of highest epidemic potential tends to be reached earlier each year. This trend deserves to be investigated further once data becomes available. These results are robust to parameter variations tested in our sensitivity analysis, following a global variance-based approach most appropriate for models with nonlinearities and interactions (Saltelli et al., 2019).

Our work is applied to Senegal, western Africa, at a larger scale than most of previous published RVF works conducted here. A previous study produced a spatial risk assessment of RVF in Senegal, at the country-level (Clements et al., 2007), using statistical methods on serology data. However, serological data points are scarce in the Ferlo region, while we did show that this region is periodically suitable for foci of infection. By using a mechanistic approach instead of a statistical one, and integrating the most trustworthy sources of input data, we build a new step towards a better understanding of the spatio-temporal dynamics of RVF in a Sahelian setting. In the absence of validation data regarding the time, location, and number of cases, the current study is not meant to directly inform decision-makers.

We provide the first mapping of RVF epidemic potential in the West African Sahel using the basic reproduction number. We achieve better spatial and temporal resolutions than previous studies in RVF-free regions (Barker et al., 2013; Fischer et al., 2013), which was made possible by the use of satellite Sentinel 2 images by Tran et al. (2019) along with ground truth validation data and a precise knowledge of temporary ponds filling dynamics. However, host densities, which do not stand out
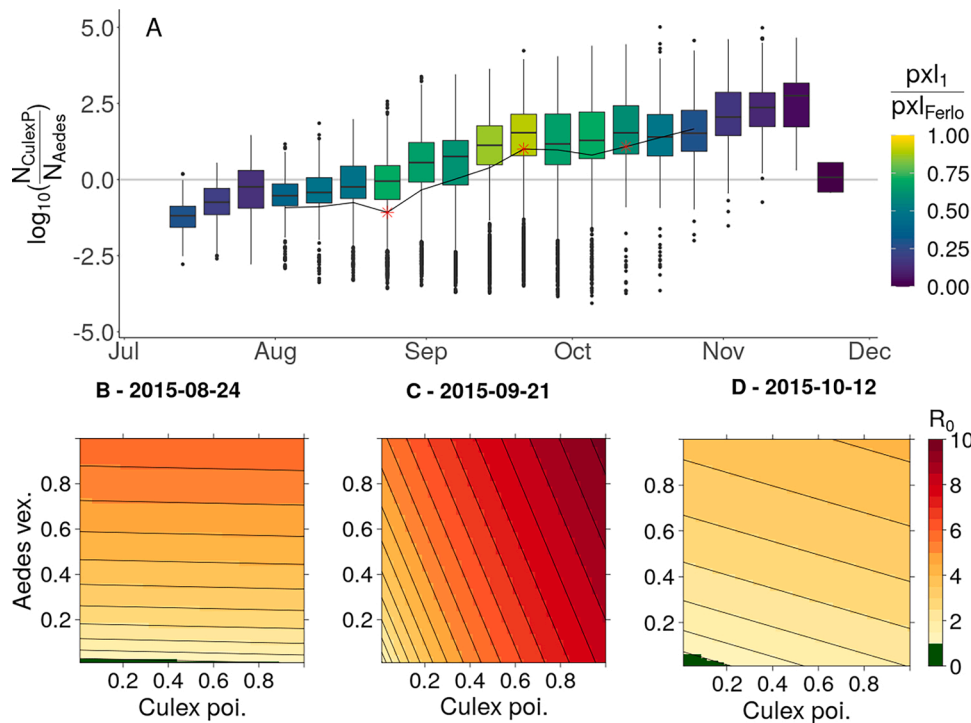
Fig. 4. Decreased vector densities do not greatly reduce RVF epidemic potential in at-risk locations. Example of Ferlo 2015. A: Relative abundance of vector populations $log_{10}(N_{C.\ poicilipes}/N_{Ae.\ v.\ arabiensis})$ within pixels having $R_0 > 1$ over time. Light grey line indicates equal densities. For boxplots, see legend of Fig. 2. Outliers are shown. Colors inside boxplots indicate the number of pixels with $R_0 > 1$ (pxl_1, min 4, max 1527) at each introduction date, normalized by the total number of pixels in the Ferlo (1702). Black line corresponds to the particular value of the ratio in Barkedji, for introduction dates inducing $R_0 > 1$. Stars are positioned at introduction dates 2015-08-24, 2015-09-21 and 2015-10-12. 2015-09-21 corresponds to the maximum pxl_1 in the Ferlo this season. The other two dates both induce $R_0 > 1$ in Barkedji but exhibit diametrically opposed vector composition. B-D: Variation of R_0 in Barkedji when decreasing vector densities, for 3 different dates of introduction. Axes represent the proportion of initial vector density applied for the R_0 computation; the reference is at the top right corner (1,1).
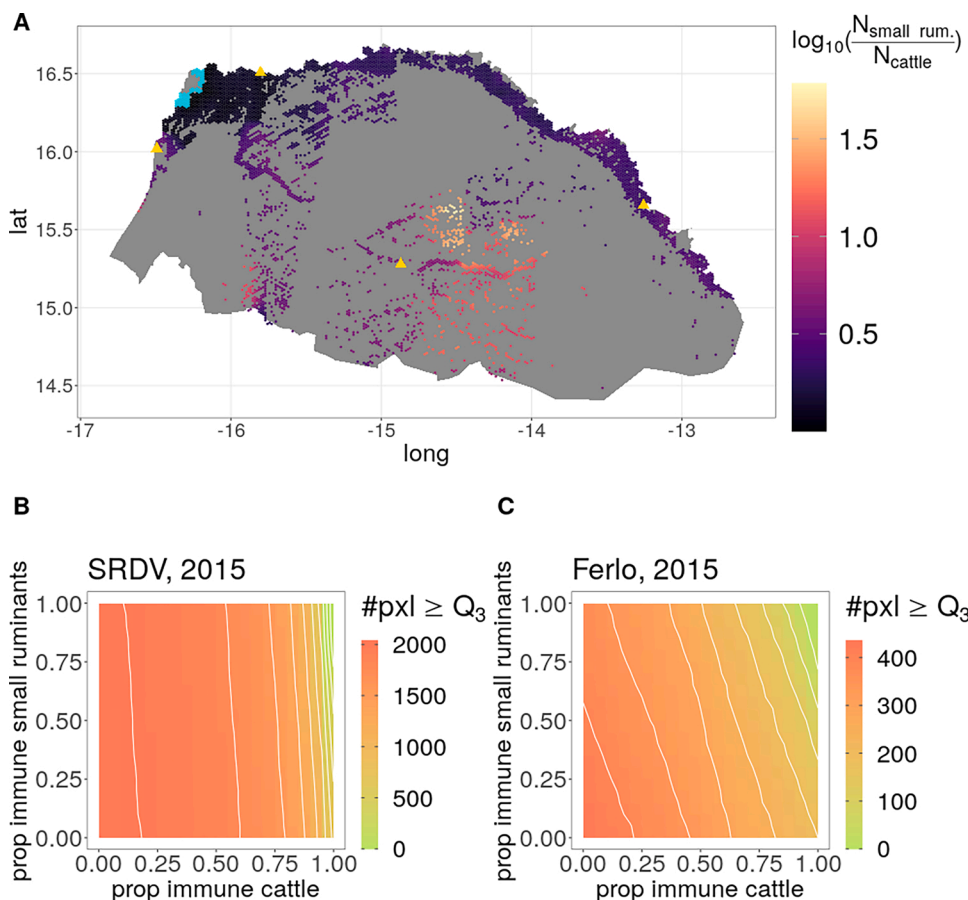
Fig. 5. In both study areas, an increase in the proportion of immune cattle decreases the number of pixels with high R_0 values ($R_0 > Q_{3,\ year}$) more effectively than increasing the proportion of immune small ruminants. A - Map of relative densities of hosts $log_{10}(N_{small\ ruminants}/N_{cattle})$ within pixels of our study area. Blue pixels have more cattle than small ruminants, the biggest difference being $log_{10}(N_{small\ ruminants}/N_{cattle})$ = -0.08. B-C – Effect of increasing host immunity on the number of pixels with $R_0 > Q_{3,\ 2015}$ by study area (B: SRDV, C: Ferlo). Axis represents the proportion of immune hosts applied for the R_0 computation. The reference is the absence of herd immunity (0,0) in the bottom left corner. (For interpretation of the references to colour in this figure legend, the reader is referred to the web version of this article.)

in our sensitivity analysis, may vary beyond the range presently allowed. Indeed, their temporal dynamics, mostly driven by animal mobility, is not incorporated into GLW 3 data, and might affect the population-specific contact rate with vectors and therefore R_0 values. Remote-sensing methods are considered a promising tool to measure human mobility (Bharti and Tatem, 2018), but we also need qualitative
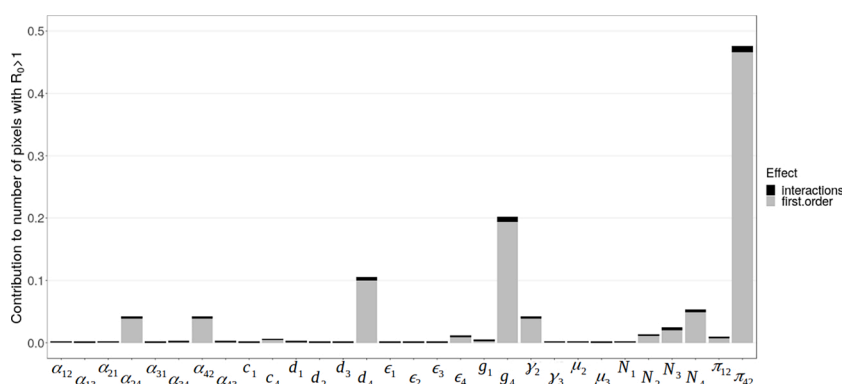
Fig. 6. The feeding preferences and the gonotrophic cycle duration of the most abundant vector species are the most influential parameters on the epidemic potential at the regional scale. Example of Ferlo, 2015. Results of the FAST sensitivity analysis showing contribution of model parameters to the maximum number of pixels with $R_0 > 1$ (pxl_1) in the season. Sensitivity indices for principal effect in grey and for interactions in black. Definition and reference values of parameters can be found in Table 1. The introduction date inducing the highest pxl_1 during the 2015 rainy season is 09-21 for 299,999 scenarios and 09-14 for one scenario (Table S.9). At these dates, C. poicilipes is on average the most abundant vector population in the Ferlo within pixels with $R_0 > 1$ (Fig. S.4).

data on factors guiding decisions of nomadic herders in order to include animal mobility in a mechanistic way (Apolloni et al., 2018; Belkhiria et al., 2019). Future work could expand our framework to longer periods of time, provided host and vector densities can be estimated, as was the case in a recent study using the same entomological model as we did, in a more constrained area (Durand et al., 2020).

The mechanistic approach used in this paper is the best suited to describe the complexity of RVF epidemic potential in our study region. Indeed, neither host nor vector densities alone are sufficient to predict the local epidemic potential, contrary to what was implied by previous mappings and statistical studies (Bicout and Sabatier, 2004; Caminade et al., 2011). It is actually the process of blood feeding, during which host and vector populations interact, which should accurately be described to achieve the most reliable estimates of RVF epidemic potential. We account for the influence of temperature in our model, which is known to strongly influence the risk of vector-borne diseases transmission (Kamiya et al., 2020; Mordecai et al., 2017, 2019). Important changes in temperature along with rainfall are expected in the future, but simulating the consequences of such changes is beyond the scope of this study. The adequate contact rate, an aggregated parameter used in previous models (Gaff et al., 2007; Mpeshe et al., 2014), is decomposed here to assess the importance of each of its components, as in Turner et al. (2013). Based on our sensitivity analysis, we recommend that future biological investigations focus on the feeding preferences of vectors and the duration of their gonotrophic cycle, in relation with temperature.

The inclusion of two host and two vector populations provides new insights on RVF epidemic potential, and this structure should be kept for future models studying RVF in the region. We show that decreased vector densities are not sufficient to limit the epidemic potential of RVF, regardless of the introduction date considered. Indeed, vector abundances are not always a good predictor of RVF epidemic potential, with high R_0 values sometimes driven by the least abundant vector population. Moreover, cattle contribute strongly to RVF transmission and their immune status is likely to influence the epidemic potential at the regional scale. Favoring vaccination of cattle over small ruminants is not what is usually done in the field. Veterinary services, along with herders, tend to promote small ruminant vaccination as they are more likely to die from the disease and thus need more protection (Sow et al., 2016). The importance of small ruminant trade, particularly around the Tabaski festival, might also justify this approach (Lancelot et al., 2019). Operational decisions regarding targeted vaccination campaigns should therefore consider the potential benefits of cattle immunity at the population scale.

In the present study, we provide a better understanding of conditions which could trigger the onset of an epidemic. However, this should be interpreted with caution, and should not be considered as an indicator of epidemic size. Indeed, multiple introductions or sudden unfavorable conditions might lead to diseases persisting with $R_0 < 1$ or dying out with $R_0 > 1$ (Li et al., 2011). In addition, our results could be used as

initial conditions for a stochastic mechanistic model of spatio-temporal transmission, which would include processes underlying epidemic dynamic after RVFV introduction, such as animal mobility. Such a model would benefit from an increased availability of epidemiological data for validation and parametrization, which are necessary to unravel the underlying mechanisms driving the spatio-temporal dynamics of RVF in the West African Sahel.

Data and code accessibility

Input data and scripts are available online: https://sourcesup.renater.fr/projects/rvf-r0-senegal/

CRediT authorship contribution statement

Hélène Cecilia: Conceptualization, Data curation, Formal analysis, Funding acquisition, Methodology, Software, Validation, Visualization, Writing - original draft, Writing - review & editing. **Raphaëlle Métras:** Conceptualization, Methodology, Supervision, Visualization, Writing - original draft, Writing - review & editing. **Assane Gueye Fall:** Resources, Writing - review & editing. **Modou Moustapha Lo:** Resources, Writing - review & editing. **Renaud Lancelot:** Conceptualization, Funding acquisition, Project administration, Supervision, Writing - review & editing. **Pauline Ezanno:** Conceptualization, Funding acquisition, Methodology, Project administration, Resources, Supervision, Validation, Visualization, Writing - original draft, Writing - review & editing.

Declaration of Competing Interest

The authors declare no conflict of interest.

Appendix A. Supplementary data

Supplementary material related to this article can be found, in the

online version, at doi:https://doi.org/10.1016/j.epidem.2020.100409.

References

Adriansen, H.K., 2008. Understanding pastoral mobility: the case of Senegalese Fulani. Geogr. J. 174 (3), 17.

Anyamba, A., Chretien, J.-P., Small, J., Tucker, C.J., Formenty, P.B., Richardson, J.H., Britch, S.C., Schnabel, D.C., Erickson, R.L., Linthicum, K.J., 2009. Prediction of a Rift Valley fever outbreak. Proc. Natl. Acad. Sci. U. S. A. 106 (3), 955–959. https://doi.org/10.1073/pnas.0806490106.

Anyangu, A.S., Gould, L.H., Sharif, S.K., Nguku, P.M., Omolo, J.O., Mutonga, D., Rao, C.Y., Lederman, E.R., Schnabel, D., Paweska, J.T., Katz, M., Hightower, A., Njenga, M.K., Feikin, D.R., Breiman, R.F., 2010. Risk factors for severe Rift Valley fever infection in Kenya, 2007. Am. J. Trop. Med. Hyg. 83, 14–21. https://doi.org/10.4269/ajtmh.2010.09-0293.

Apolloni, A., Nicolas, G., Coste, C., EL Mamy, A.B., Yahya, B., EL Arbi, A.S., Gueya, M.B., Baba, D., Gilbert, M., Lancelot, R., 2018. Towards the description of livestock mobility in Sahelian Africa: some results from a survey in Mauritania. PLoS One 13 (1). https://doi.org/10.1371/journal.pone.0191565 e0191565.

Ba, Y., Diallo, D., Kebe, C.M.F., Dia, I., Diallo, M., 2005. Aspects of bioecology of two Rift Valley fever virus vectors in Senegal (West Africa): Aedes vexans and Culex poicilipes (Diptera: Culicidae). J. Med. Entomol. 42 (5), 12.

Ba, Y., Diallo, D., Dia, I., Diallo, M., 2006. Comportement trophique des vecteurs du virus de la fièvre de la vallée du Rift au Sénégal : implications dans l'épidémiologie de la maladie. Bull. Soc. Pathol. Exot. 99 (4), 283–289.

Barker, C.M., Niu, T., Reisen, W.K., Hartley, D.M., 2013. Data-driven modeling to assess receptivity for Rift Valley fever virus. PLoS Negl. Trop. Dis. 7 (11), e2515. https://doi.org/10.1371/journal.pntd.0002515.

Belkhiria, J., Lo, M.M., Sow, F., Martínez-López, B., Chevalier, V., 2019. Application of exponential random graph models to determine nomadic herders' movements in Senegal. Transbound. Emerg. Dis. 66, 1642–1652. https://doi.org/10.1111/tbed.13198.

Bharti, N., Tatem, A.J., 2018. Fluctuations in anthropogenic nighttime lights from satellite imagery for five cities in Niger and Nigeria. Sci. Data 5, 180256. https://doi.org/10.1038/sdata.2018.256.

Bicout, D.J., Sabatier, P., 2004. Mapping Rift Valley fever vectors and prevalence using rainfall variations. Vector Borne Zoonotic Dis. 4 (1), 33–42. https://doi.org/10.1089/153036604773082979.

Bird, B.H., Ksiazek, T.G., Nichol, S.T., MacLachlan, N.J., 2009. Rift Valley fever virus. J. Am. Vet. Med. Assoc. 234 (7), 883–893.

Biteye, B., Fall, A.G., Ciss, M., Seck, M.T., Apolloni, A., Fall, M., Tran, A., Gimonneau, G., 2018. Ecological distribution and population dynamics of Rift Valley fever virus mosquito vectors (Diptera, Culicidae) in Senegal. Parasit. Vectors 11 (1), 27. https://doi.org/10.1186/s13071-017-2591-9.

Bop, M., Amadou, A., Seidou, O., Kébé, C.M.F., Ndione, J.A., Sambou, S., Sanda, I.S., 2014. Modeling the hydrological dynamic of the breeding water bodies in Barkedji's zone. J. Water Resource Prot. 06 (08), 741–755. https://doi.org/10.4236/jwarp.2014.68071.

Bruckmann, L., 2018. Crue et développement rural dans la vallée du Sénégal : entre marginalisation et résilience. Belgeo 2. https://doi.org/10.4000/belgeo.23158.

Calisher, C.H., 2000. West Nile virus in the new world: appearance, persistence, and adaptation to a new econiche—an opportunity taken. Viral Immunol. 13 (4), 411–414. https://doi.org/10.1089/vim.2000.13.411.

Caminade, C., Ndione, J.A., Kebe, C.M.F., Jones, A.E., Danuor, S., Tay, S., Tourre, Y.M., Lacaux, J.-P., Vignolles, C., Duchemin, J.B., Jeanne, I., Morse, A.P., 2011. Mapping Rift Valley fever and malaria risk over West Africa using climatic indicators. Atmos. Sci. Lett. 12 (1), 96–103. https://doi.org/10.1002/asl.296.

Caminade, C., Ndione, J., Diallo, M., MacLeod, D., Faye, O., Ba, Y., Dia, I., Morse, A., 2014. Rift Valley fever outbreaks in Mauritania and related environmental conditions. Int. J. Environ. Res. Public Health 11 (1), 903–918. https://doi.org/10.3390/ijerph110100903.

Cavalerie, L., Charron, M.V.P., Ezanno, P., Dommergues, L., Zumbo, B., Cardinale, E., 2015. A stochastic model to study Rift Valley fever persistence with different seasonal patterns of vector abundance: new insights on the endemicity in the tropical island of Mayotte. PLoS One 10 (7). https://doi.org/10.1371/journal.pone.0130838 e0130838.

Chevalier, V., Pépin, M., Plée, L., Lancelot, R., 2010. Rift Valley fever - a threat for Europe? Clin. Microbiol. Infect. 19 (8), 705–708. https://doi.org/10.1111/1469-0691.12163.

Clements, A.C., Pfeiffer, D.U., Martin, V., Pittiglio, C., Best, N., Thiongane, Y., 2007. Spatial risk assessment of rift valley fever in Senegal. Vector-borne Zoonotic Dis. 7 (2), 203–216. https://doi.org/10.1089/vbz.2006.0600.

Danzetta, M.L., Bruno, R., Sauro, F., Savini, L., Calistri, P., 2016. Rift Valley fever transmission dynamics described by compartmental models. Prev. Vet. Med. 134, 197–210. https://doi.org/10.1016/j.prevetmed.2016.09.007.

Davies, F.G., Martin, V., 2003. Recognizing Rift Valley fever. FAO Animal Health Manual 17.

Diallo, M., Lochouarn, L., Ba, K., Sall, A.A., Mondo, M., Girault, L., Mathiot, C., 2000. First isolation of the Rift Valley fever virus from Culex poicilipes (Diptera: culicidae) in nature. Am. J. Trop. Med. Hyg. 62 (6), 702–704. https://doi.org/10.4269/ajtmh.2000.62.702.

Diallo, D., Talla, C., Ba, Y., Dia, I., Sall, A.A., Diallo, M., 2011. Temporal distribution and spatial pattern of abundance of the Rift Valley fever and West Nile fever vectors in Barkedji, Senegal. Journal of Vector Ecology 36 (2), 426–436. https://doi.org/10.1111/j.1948-7134.2011.00184.x.

Durand, B., Lo Modou, M., Tran, A., Ba, A., Sow, F., Belkhiria, J., Fall, A.G., Biteye, B., Grosbois, V., Chevalier, V., 2020. Rift Valley fever in northern Senegal: a modelling approach to analyse the processes underlying virus circulation recurrence. PLoS Negl. Trop. Dis. 14 (6) https://doi.org/10.1371/journal.pntd.0008009 e0008009.

EMPRES, 2003. Early Warning Message: Rift Valley Fever in the Gambia; Tabaski Is Approaching. URL (Accessed 17 February 2020). http://www.fao.org/AG/AGAInfo/programmes/en/empres/earlywarning/ew14.html.

Fall, A.G., Diaïté, A., Lancelot, R., Tran, A., Soti, V., Etter, E., Konaté, L., Faye, O., Bouyer, J., 2011. Feeding behaviour of potential vectors of West Nile virus in Senegal. Parasit. Vectors 4 (1), 99. https://doi.org/10.1186/1756-3305-4-99.

Fall, A., Diaïté, A., Seck, M., Bouyer, J., Lefrançois, T., Vachiéry, N., Aprelon, A., Faye, O., Konaté, L., Lancelot, R., 2013. West Nile virus transmission in sentinel chickens and potential mosquito vectors, Senegal River delta, 2008–2009. Int. J. Environ. Res. Public Health 10 (10), 4718–4727. https://doi.org/10.3390/ijerph10104718.

Fischer, E.A., Boender, G.-J., Nodelijk, G., de Koeijer, A.A., van Roermund, H.J., 2013. The transmission potential of Rift Valley fever virus among livestock in the Netherlands: a modelling study. Vet. Res. 44 (1), 58. https://doi.org/10.1186/1297-9716-44-58.

Fontenille, D., Traore-Laminaza, M., Diallo, M., Thonnon, J., Digoutte, J.P., Zeller, H.G., 1998. New vectors of Rift Valley fever in West Africa. Emerging Infect. Dis. 4 (2), 289–293. https://doi.org/10.3201/eid0402.980218.

Gaff, H.D., Hartley, D.M., Leahy, N.P., 2007. An epidemiological model of Rift Valley fever. Electronic Journal of Differential Equations 2007 (115), 1–12.

Gerdes, G.H., 2004. Rift Valley fever. Rev. sci. tech. Off. int. Epiz. 23 (2), 613–623.

Gilbert, M., Nicolas, G., Cinardi, G., Van Boeckel, T.P., Vanwambeke, S.O., Wint, G.R.W., Robinson, T.P., 2018. Global distribution data for cattle, buffaloes, horses, sheep, goats, pigs, chickens and ducks in 2010. Sci. Data 5, 180227. https://doi.org/10.1038/sdata.2018.227.

Gubbins, S., Carpenter, S., Baylis, M., Wood, J.L., Mellor, P.S., 2008. Assessing the risk of bluetongue to UK livestock: uncertainty and sensitivity analyses of a temperature-dependent model for the basic reproduction number. J. R. Soc. Interface 5 (20), 363–371. https://doi.org/10.1098/rsif.2007.1110.

Hammami, P., Lancelot, R., Lesnoff, M., 2016. Modelling the dynamics of post-vaccination immunity rate in a population of Sahelian sheep after a vaccination campaign against Peste des Petits Ruminants virus. PLoS One 11 (9). https://doi.org/10.1371/journal.pone.0161769 e0161769.

Hartemink, N.A., Randolph, S.E., Davis, S.A., Heesterbeek, J.A.P., 2008. The basic reproduction number for complex disease systems: defining R_0 for tick-borne infections. Am. Nat. 171 (6), 743–754. https://doi.org/10.1086/587530.

Jupp, P.G., Kemp, A., Grobbelaar, A., Leman, P., Burt, F.J., Alahmed, A.M., Mujalli, D.A., Khamees, M.A., Swanepoel, R., 2002. The 2000 epidemic of Rift Valley fever in Saudi Arabia: mosquito vector studies. Med. Vet. Entomol. 16 (3), 245–252. https://doi.org/10.1046/j.1365-2915.2002.00371.x.

Kamiya, T., Greischar, M.A., Wadhawan, K., Gilbert, B., Paaijmans, K., Mideo, N., 2020. Temperature-dependent variation in the extrinsic incubation period elevates the risk of vector-borne disease emergence. Epidemics 30, 100382. https://doi.org/10.1016/j.epidem.2019.100382.

Kim, Y., Dommergues, L., M'sa, A.B., Mérot, P., Cardinale, E., Edmunds, J., Pfeiffer, D., Fournié, G., Métras, R., 2018. Livestock trade network: potential for disease transmission and implications for risk-based surveillance on the island of Mayotte. Sci. Rep. 8, 11550. https://doi.org/10.1038/s41598-018-29999-y.

Lacaux, J., Tourre, Y., Vignolles, C., Ndione, J., Lafaye, M., 2007. Classification of ponds from high-spatial resolution remote sensing: application to Rift Valley fever epidemics in Senegal. Remote Sens. Environ. 106 (1), 66–74. https://doi.org/10.1016/j.rse.2006.07.012.

Lancelot, R., Cêtre-Sossah, C., Hassan, O.A., Yahya, B., Ould Elmamy, B., Fall, A.G., Lo, M.M., Apolloni, A., Arsevska, E., Chevalier, V., 2019. Rift Valley fever: One Health at play? In: Kardjadj, M., Diallo, A., Lancelot, R. (Eds.), Transboundary Animal Diseases in Sahelian Africa and Connected Regions. Springer International Publishing, Cham, pp. 121–148. https://doi.org/10.1007/978-3-030-25385-1_8. ISBN 978-3-030-25384-4 978-3-030-25385-1.

Laughlin, L.W., Meegan, J.M., Strausbaugh, L.J., Morens, D.M., Watten, R.H., 1979. Epidemic Rift Valley fever in Egypt: observations of the spectrum of human illness. Trans. R. Soc. Trop. Med. Hyg. 73 (6), 630–633. https://doi.org/10.1016/0035-203(79)90006-3.

Li, J., Blakeley, D., Smith, R.J., 2011. The failure of R0. Comput. Math. Methods Med. 17 https://doi.org/10.1155/2011/527610, 2011.

Linthicum, K.J., Davies, F.G., Kairo, A., Bailey, C.L., 1985. Rift Valley fever virus (family Bunyaviridae, genus Phlebovirus). Isolations from Diptera collected during an inter-epizootic period in Kenya. J. Hyg. (Lond) 95 (01), 197–209. https://doi.org/10.1017/S0022172400062434.

Linthicum, K.J., Britch, S.C., Anyamba, A., 2016. Rift Valley fever: an emerging mosquito-borne disease. Annu. Rev. Entomol. 61 (1), 395–415. https://doi.org/10.1146/annurev-ento-010715-023819.

Lumley, S., Horton, D.L., Hernandez-Triana, L.L.M., Johnson, N., Fooks, A.R., Hewson, R., 2017. Rift Valley fever virus: strategies for maintenance, survival and vertical transmission in mosquitoes. J. Gen. Virol. 98 (5), 875–887. https://doi.org/10.1099/jgv.0.000765.

Madani, T.A., Al-Mazrou, Y.Y., Al-Jeffri, M.H., Mishkhas, A.A., Al-Rabeah, A.M., Turkistani, A.M., Al-Sayed, M.O., Abodahish, A.A., Khan, A.S., Ksiazek, T.G., Shobokshi, O., 2003. Rift Valley fever epidemic in Saudi Arabia: epidemiological, clinical, and laboratory characteristics. Clin. Infect. Dis. 37 (8), 1084–1092. https://doi.org/10.1086/378747.

Madder, D., Surgeoner, G., Helson, B., 1983. Number of generations, egg production, and developmental time of Culex pipiens and Culex restuans (Diptera: Culicidae) in

Southern Ontario. J. Med. Entomol. 20 (3), 275–287. https://doi.org/10.1093/jmedent/20.3.275.

Mehand, M.S., Al-Shorbaji, F., Millett, P., Murgue, B., 2018. The WHO R&D Blueprint: 2018 review of emerging infectious diseases requiring urgent research and development efforts. Antiviral Res. 159, 63–67. https://doi.org/10.1016/j.antiviral.2018.09.009.

Metras, R., Collins, L.M., White, R.G., Alonso, S., Chevalier, V., Thuranira-McKeever, C., Pfeiffer, D.U., 2011. Rift Valley fever epidemiology, surveillance, and control: what have models contributed? Vector-borne Zoonotic Dis. 11 (6), 761–771. https://doi.org/10.1089/vbz.2010.0200.

Mondet, B., Diaïté, A., Ndione, J.-A., Fall, A.G., Chevalier, V., Lancelot, R., Ndiaye, M., Ponçon, N., 2005. Rainfall patterns and population dynamics of Aedes (Aedimorphus) vexans arabiensis, Patton 1905 (Diptera: Culicidae), a potential vector of Rift Valley fever virus in Senegal. J. Vector Ecol. 30 (1), 5.

Mordecai, E.A., Cohen, J.M., Evans, M.V., Gudapati, P., Johnson, L.R., Lippi, C.A., Miazgowicz, K., Murdock, C.C., Rohr, J.R., Ryan, S.J., Savage, V., Shocket, M.S., Ibarra, A.S., Thomas, M.B., Weikel, D.P., 2017. Detecting the impact of temperature on transmission of Zika, dengue, and chikungunya using mechanistic models. PLoS Negl. Trop. Dis. 11 (4) e0005568.

Mordecai, E.A., Caldwell, J.M., Grossman, M.K., Lippi, C.A., Johnson, L.R., Neira, M., Rohr, J.R., Ryan, S.J., Savage, V., Shocket, M.S., Sippy, R., Stewart Ibarra, A.M., Thomas, M.B., Villena, O., 2019. Thermal biology of mosquito-borne disease. Ecol. Lett. https://doi.org/10.1111/ele.13335.

Mpeshe, S.C., Luboobi, L.S., Nkansah-Gyekye, Y., 2014. Modeling the impact of climate change on the dynamics of Rift Valley fever. Comput. Math. Methods Med. 12 https://doi.org/10.1155/2014/627586, 2014.

Ndiaye, E.H., Fall, G., Gaye, A., Bob, N.S., Talla, C., Diagne, C.T., Diallo, D., Ba, Y., Dia, I., Kohl, A., Sall, A.A., Diallo, M., 2016. Vector competence of Aedes vexans (Meigen), Culex poicilipes (Theobald) and Cx. quinquefasciatus Say from Senegal for West and East African lineages of Rift Valley fever virus. Parasit. Vectors 9, 94. https://doi.org/10.1186/s13071-016-1383-y.

Ndione, J.-A., Diop, M., Lacaux, J.-P., Gaye, A.T., 2008. Variabilité intra-saisonnière de la pluviométrie et émergence de la fièvre de la Vallée du Rift dans la vallée du fleuve Sénégal : nouvelles considérations. Climatologie (5), 83–97. https://doi.org/10.4267/climatologie.794.

Ndione, J.-A., Lacaux, J.-P., Tourre, Y., Vignolles, C., Fontanaz, D., Lafaye, M., 2009. Mares temporaires et risques sanitaires au Ferlo: contribution de la télédétection pour l'étude de la fièvre de la Vallée du Rift entre août 2003 et janvier 2004. Secheresse 20 (1), 153–160. https://doi.org/10.1684/sec.2009.0170.

Nicolas, G., Chevalier, V., Tantely, L.M., Fontenille, D., Durand, B., 2014. A spatially explicit metapopulation model and cattle trade analysis suggests key determinants for the recurrent circulation of Rift Valley fever virus in a pilot area of Madagascar highlands. PLoS Negl. Trop. Dis. 8 (12), e3346. https://doi.org/10.1371/journal.pntd.0003346.

Niu, T., Gaff, H.D., Papelis, Y.E., Hartley, D.M., 2012. An epidemiological model of Rift Valley fever with spatial dynamics. Comput. Math. Methods Med. 12 https://doi.org/10.1155/2012/138757, 2012.

Parham, P.E., Waldock, J., Christophides, G.K., Hemming, D., Agusto, F., Evans, K.J., Fefferman, N., Gaff, H., Gumel, A., LaDeau, S., Lenhart, S., Mickens, R.E., Naumova, E.N., Ostfeld, R.S., Ready, P.D., Thomas, M.B., Velasco-Hernandez, J., Michael, E., 2015. Climate, environmental and socio-economic change: weighing up the balance in vector-borne disease transmission. Philos. Trans. Biol. Sci. 370, 20130551 https://doi.org/10.1098/rstb.2013.0551.

Pedro, S.A., Abelman, S., Tonnang, H.E.Z., 2016. Predicting Rift Valley fever inter-epidemic activities and outbreak patterns: insights from a stochastic host-vector model. PLoS Negl. Trop. Dis. 10 (12) https://doi.org/10.1371/journal.pntd.0005167 e0005167.

Pepin, M., Bouloy, M., Bird, B.H., Kemp, A., Paweska, J., 2010. Rift Valley fever virus (Bunyaviridae: Phlebovirus): an update on pathogenesis, molecular epidemiology,

vectors, diagnostics and prevention. Vet. Res. 41 (6), 61. https://doi.org/10.1051/vetres/2010033.

Saltelli, A., Chan, R., Scott, F.M., 2008. Sensitivity Analysis. Wiley. ISBN 978-0-470-74382-74389.

Saltelli, A., Aleksankina, K., Becker, W., Fennell, P., Ferretti, F., Holst, N., Li, S., Wu, Q., 2019. Why so many published sensitivity analyses are false: a systematic review of sensitivity analysis practices. Environ. Model. Softw. 114, 29–39. https://doi.org/10.1016/j.envsoft.2019.01.012.

Soti, V., Puech, C., Lo Seen, D., Bertran, A., Vignolles, C., Mondet, B., Dessay, N., Tran, A., 2010. The potential for remote sensing and hydrologic modelling to assess the spatio-temporal dynamics of ponds in the Ferlo Region (Senegal). Hydrol. Earth Syst. Sci. 14 (8), 1449–1464. https://doi.org/10.5194/hess-14-1449-2010.

Soti, V., Chevalier, V., Maura, J., Bégué, A., Lelong, C., Lancelot, R., Thiongane, Y., Tran, A., 2013. Identifying landscape features associated with Rift Valley fever virus transmission, Ferlo region, Senegal, using very high spatial resolution satellite imagery. Int. J. Health Geogr. 12, 10. https://doi.org/10.1186/1476-072X-12-10.

Sow, A., Faye, O., Ba, Y., Diallo, D., Fall, G., Faye, O., Bob, N.S., Loucoubar, C., Richard, V., Dia, A.T., Diallo, M., Malvy, D., Sall, A.A., 2016. Widespread Rift Valley fever emergence in Senegal in 2013–2014. Open Forum Infect. Dis. https://doi.org/10.1093/ofid/ofw149.

Spickler, A.R., 2015. Rift Valley Fever. URL (Accessed 17 February 2020). http://www.cfsph.iastate.edu/Factsheets/pdfs/rift_valley_fever.pdf.

Talla, C., Diallo, D., Dia, I., Ba, Y., Ndione, J.-A., Morse, A.P., Diop, A., Diallo, M., 2016. Modelling hotspots of the two dominant Rift Valley fever vectors (Aedes vexans and Culex poicilipes) in Barkédji, Sénégal. Parasit. Vectors 9, 111. https://doi.org/10.1186/s13071-016-1399-3.

Tourre, Y.M., Lacaux, J.-P., Vignolles, C., Lafaye, M., 2009. Climate impacts on environmental risks evaluated from space: a conceptual approach to the case of Rift Valley fever in Senegal. Glob. Health Action 2 (1), 2053. https://doi.org/10.3402/gha.v2i0.2053.

Tran, A., Trevennec, C., Lutwama, J., Sserugga, J., Gély, M., Pittiglio, C., Pinto, J., Chevalier, V., 2016. Development and assessment of a geographic knowledge-based model for mapping suitable areas for Rift Valley fever transmission in Eastern Africa. PLoS Negl. Trop. Dis. 10 (9) https://doi.org/10.1371/journal.pntd.0004999 e0004999.

Tran, A., Fall, A.G., Biteye, B., Ciss, M., Gimonneau, G., Castets, M., Seck, M.T., Chevalier, V., 2019. Spatial modeling of mosquito vectors for Rift Valley fever virus in northern Senegal: integrating satellite-derived meteorological estimates in population dynamics models. Remote Sens. (Basel) 11, 1024. https://doi.org/10.3390/rs11091024.

Turner, J., Bowers, R.G., Baylis, M., 2013. Two-host, two-vector basic reproduction ratio (R0) for Bluetongue. PLoS One 8 (1), e53128. https://doi.org/10.1371/journal.pone.0053128.

van den Driessche, P., Watmough, J., 2002. Reproduction numbers and sub-threshold endemic equilibria for compartmental models of disease transmission. Math. Biosci. 180 (1-), 29–48. https://doi.org/10.1016/S0025-5564(02)00108-6, 2.

Vignolles, C., Lacaux, J.-P., Tourre, Y.M., Bigeard, G., Ndione, J.-A., Lafaye, M., 2009. Rift Valley fever in a zone potentially occupied by Aedes vexans in Senegal: dynamics and risk mapping. Geospat. Health 3 (2), 211–220. https://doi.org/10.4081/gh.2009.221.

Wonham, M.J., Lewis, M.A., Renclawowicz, J., van den Driessche, P., 2006. Transmission assumptions generate conflicting predictions in host-vector disease models: a case study in West Nile virus. Ecol. Lett. 9 (6), 706–725. https://doi.org/10.1111/j.1461-0248.2006.00912.x.

World Health Organization (WHO), 2014. A Global Brief on Vector-borne Diseases http://apps.who.int/iris/bitstream/10665/111008/1/WHO_DCO_WH-D_2014.1_eng.pdf. URL (Accessed 17 February 2020).

Xue, L., Scoglio, C., 2013. The network level reproduction number for infectious diseases with both vertical and horizontal transmission. Math. Biosci. 243 (1), 67–80. https://doi.org/10.1016/j.mbs.2013.02.004.